CrystEngComm

ROYAL SOCIETY OF CHEMISTRY

PAPER

View Article Online
View Journal | View Issue

Cite this: *CrystEngComm*, 2021, **23**, 7963

Effects of growth substrate on the nucleation of monolayer $MoTe_2$†

David J. Hynek,[a] Raivat M. Singhania,[b] James L. Hart,[a] Benjamin Davis,[b] Mengjing Wang,[a] Nicholas C. Strandwitz[b] and Judy J. Cha *[a]

Received 24th February 2021,
Accepted 27th March 2021

DOI: 10.1039/d1ce00275a

rsc.li/crystengcomm

The discovery and characterization of two-dimensional (2D) materials beyond graphene has increased dramatically over the past decade with increasingly fine control over the growth dynamics of these materials. $MoTe_2$ represents a model material for studying phase change properties of 2D materials due to small energy differences between its 2H semiconducting phase and 1T′ semimetallic phase. Although some substrates are demonstrated to be better than others for the wafer-scale growth of high quality $MoTe_2$ films, substrate effects on the nucleation and growth of $MoTe_2$ are still not well understood. Here, we grow monolayer $MoTe_2$ by converting MoO_x thin films deposited on three different substrates: sapphire Al_2O_3 (0001), amorphous SiO_2, and amorphous AlO_x, and examine the early stages of the conversion reaction to elucidate the substrate effects on the nucleation of $MoTe_2$. We observe that the chemical composition of the substrate is more important than the surface topography and crystallinity of the substrate, with high quality monolayer 2H $MoTe_2$ formed on both Al_2O_3 (0001) and AlO_x in contrast to mixed phase 2H/1T′ $MoTe_2$ formed on SiO_2, as determined by Raman spectroscopy, X-ray photoelectron spectroscopy, and atomic force microscopy.

Introduction

Due to their low-dimensionality and layer-dependent properties, 2D materials have been heavily studied in recent years for their potential applications that range from catalysis[1] to energy storage.[2] Transition metal dichalcogenides (TMDCs) of the form MX_2 (M: Mo, W; X: S, Se, Te) represent a particularly heavily studied subset of 2D materials due to the wide variety of electronic phases readily accessible, expanding their uses in next-generation electronics. Of these TMDCs, $MoTe_2$ has gained recent attention for potential applications in phase-change memory and low power electronics due to small free energy differences between its semiconducting 2H (α) phase and semimetallic 1T′ (β) phase at room temperature,[3] and between semimetallic 1T′ (β) phase and topological T_d (γ) phase at low temperatures.[4,5] Many studies have shown useful physical characteristics including superconductivity,[6–8] a possible quantum spin Hall state,[9] and reversible phase switching,[10–12] yet, reliable large-scale growth of $MoTe_2$ with thickness control and high crystallinity has remained a challenge.

Several physical and electrical characterization studies have been carried out using $MoTe_2$ flakes obtained by exfoliation or chemical vapor deposition (CVD),[8,13,14] but these methods suffer from low yield and a lack of scalability. We have recently demonstrated synthesis of thickness-controlled $MoTe_2$ films through the tellurization of MoO_x ($2 < x < 3$) thin films deposited by atomic layer deposition (ALD), where the number of ALD cycles determined the thickness of the $MoTe_2$ films.[15] The $MoTe_2$ films were uniform across a wafer scale and could be synthesized on Al_2O_3 (0001) down to a monolayer. In this work, we examined the effects of substrate composition and structure on the nucleation and crystallinity of $MoTe_2$ thin films when $MoTe_2$ was converted from ALD-deposited MoO_x thin films. To determine how the growth of $MoTe_2$ is affected by the chemical composition or crystallinity of the underlying substrate, we utilized the following substrates: sapphire Al_2O_3 (0001), 3 nm-thick ALD-deposited amorphous AlO_x on SiO_2/Si, and amorphous SiO_2. We show that the complete conversion from MoO_x to monolayer 2H $MoTe_2$ can be achieved on both Al_2O_3 (0001) and amorphous AlO_x while only mixed phase 2H/1T′ films were realized on amorphous SiO_2. Our results indicate that chemical composition plays a more important role than the crystallinity or surface topography of the growth substrate.

[a] *Energy Sciences Institute, Department of Mechanical Engineering and Materials Science, Yale University, West Haven, CT 06516, USA. E-mail: judy.cha@yale.edu*
[b] *Department of Materials Science and Engineering, Lehigh University, Bethlehem, PA 18015, USA*

† Electronic supplementary information (ESI) available. See DOI: 10.1039/d1ce00275a

Results and discussion

Amorphous MoO_x films were deposited by ALD on sapphire Al_2O_3 (0001), 3 nm-thick ALD-deposited amorphous AlO_x, and amorphous SiO_2 (Methods). Based on our previous study,[15] MoO_x thin films of 8 and 10 ALD cycles were chosen to grow monolayer $MoTe_2$ in order to maximize the effects of the substrate on the crystalline quality of $MoTe_2$ while a MoO_x film of 120 ALD cycles was used to grow a thick $MoTe_2$ for transmission electron microscopy (TEM) characterization. The oxide films were tellurized in a two-zone furnace under an H_2/Ar atmosphere at 600 °C for three different time intervals: 15 minutes, 20 minutes, and 50 minutes (Fig. 1e, see Methods for synthesis details). This 8–10 cycle synthesis resulted in a discontinuous, polycrystalline film (Fig. S1a and b†), where the individual domains consisted of monolayer 2H $MoTe_2$, with an average domain size of 10–20 nm. The discontinuity observed in $MoTe_2$ is due to the fact that 8 and 10 ALD cycle MoO_x films were not sufficiently thick to form a continuous monolayer. Uniform and continuous 2H $MoTe_2$ films were obtained using the 120 ALD cycle MoO_x films deposited on amorphous AlO_x (Fig. 1f and g). The selected area electron diffraction and high-resolution TEM images confirm the 2H phase for $MoTe_2$.

The evolution of the crystalline phase of the $MoTe_2$ films on the three different substrates was tracked throughout the length of the 50 minute reaction after three different time intervals (15 minutes, 20 minutes, and 50 minutes) using Raman spectroscopy (Fig. 2) (Methods). The 2H phase is characterized by two main modes at 170 cm^{-1} (A_{1g}) and 234 cm^{-1} ($E_{2g}{}^1$),[16–18] while the 1T′ phase is characterized by a primary mode at 163 cm^{-1} ($A_g{}^4$).[19] For $MoTe_2$ synthesis, it is known that the 1T′ phase is initially synthesized due to the Te- deficient stoichiometry and a 2H phase can nucleate out of the 1T′ phase with the continual supply of Te vapor[3,15] (Fig. S2†). After a 15 minute growth, only the 8 cycle-thick MoO_x film on amorphous AlO_x has converted fully to 2H $MoTe_2$, while the $MoTe_2$ on Al_2O_3 (0001) and amorphous SiO_2 shows a mixed phase of 2H and 1T′. After 20 minutes of growth, $MoTe_2$ on the Al_2O_3 (0001) substrate has also fully converted to 2H, while the $MoTe_2$ on amorphous SiO_2 still remains mixed-phase. From 20 to 50 minutes of growth, the growth result did not change substantially, with $MoTe_2$ on the AlO_x and Al_2O_3 (0001) substrates remaining in the 2H phase, and $MoTe_2$ on the SiO_2 not converting fully to the 2H phase (Fig. 2d). We observe the same trend when 10 cycle-thick MoO_x films were converted to $MoTe_2$ on the three substrates (Fig. S3†).

The progression of the $MoTe_2$ films from MoO_x is further characterized using X-ray photoelectron spectroscopy (XPS) (Fig. 3). Mo has two primary peaks at 228 eV ($3d_{5/2}$) and 231 eV ($3d_{3/2}$),[20] with Mo-oxide peaks at slightly higher binding energies. By tracking the intensity of the oxide peaks as a function of reaction time, the reaction time needed to transform MoO_x to $MoTe_2$ was determined for each substrate. In agreement with the Raman results, after 15 minutes of reaction, $MoTe_2$ converted on the amorphous AlO_x substrate is shown to have the least amount of oxidized Mo. $MoTe_2$ converted on Al_2O_3 (0001) and amorphous SiO_2 substrates still show significant amounts of Mo-oxide peaks, suggesting incomplete conversion to $MoTe_2$. After 20 minutes of reaction, all films show almost a complete reduction in Mo-oxide peaks, with little change from 20 to 50 minutes of reaction. Interestingly, a residual amount of MoO_x remains in the $MoTe_2$ films converted on the amorphous SiO_2 and amorphous AlO_x substrates, with a higher concentration evident in the SiO_2 substrate, and no residual oxidation is observed in the $MoTe_2$ converted on sapphire (Fig. 3d). This residual MoO_x may be from surface oxidation of $MoTe_2$, or due to non van der Waals bonding at the interface between $MoTe_2$ and the two amorphous substrates. If the residual MoO_x were from the surface oxidation of $MoTe_2$, the MoO_x peaks should be present for $MoTe_2$ on all three substrates, which is not the case. Thus, the residual MoO_x observed for the two amorphous substrates cannot be attributed to the surface oxidation of $MoTe_2$. This hypothesis is further supported by very little oxidation in the Te peaks for all three substrates after 50 minutes of reaction (Fig. S4†). The absence of the oxide peaks for $MoTe_2$ converted on Al_2O_3 (0001) thus suggests that the residual MoO_x is either from the chemical bonds of $MoTe_2$ to the amorphous oxide substrates or from the diffusion of Mo atoms into the amorphous oxide substrates.

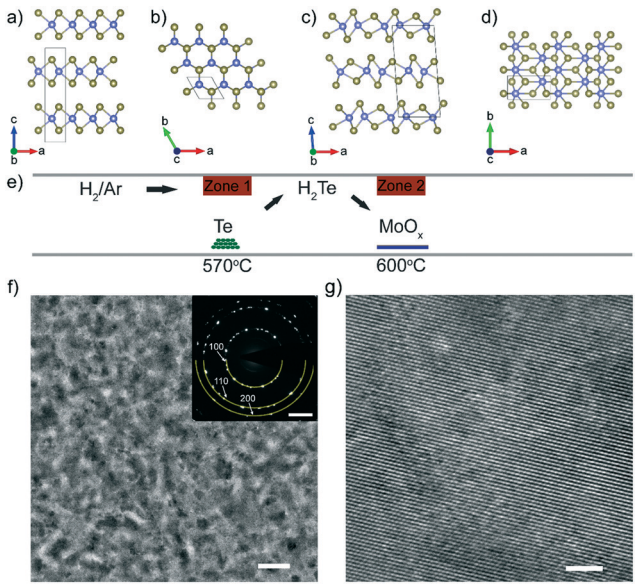

Fig. 1 Growth of 2H $MoTe_2$ converted from MoO_x thin films. a and b) 2H $MoTe_2$ viewed along *b*- and *c*-axis. c and d) 1T′ $MoTe_2$ viewed along *b*- and *c*-axis. e) Two-zone furnace growth schematic. f) TEM image taken along the *c*-axis, showing a 2H $MoTe_2$ film, converted from 120 ALD cycle-thick MoO_x grown on 3 nm-thick amorphous AlO_x. Scale bar, 100 nm. (Inset) selected area electron diffraction from (f). Scale bar, 10 nm^{-1}. g) High resolution TEM image of the film shown in (f). Scale bar, 3 nm.

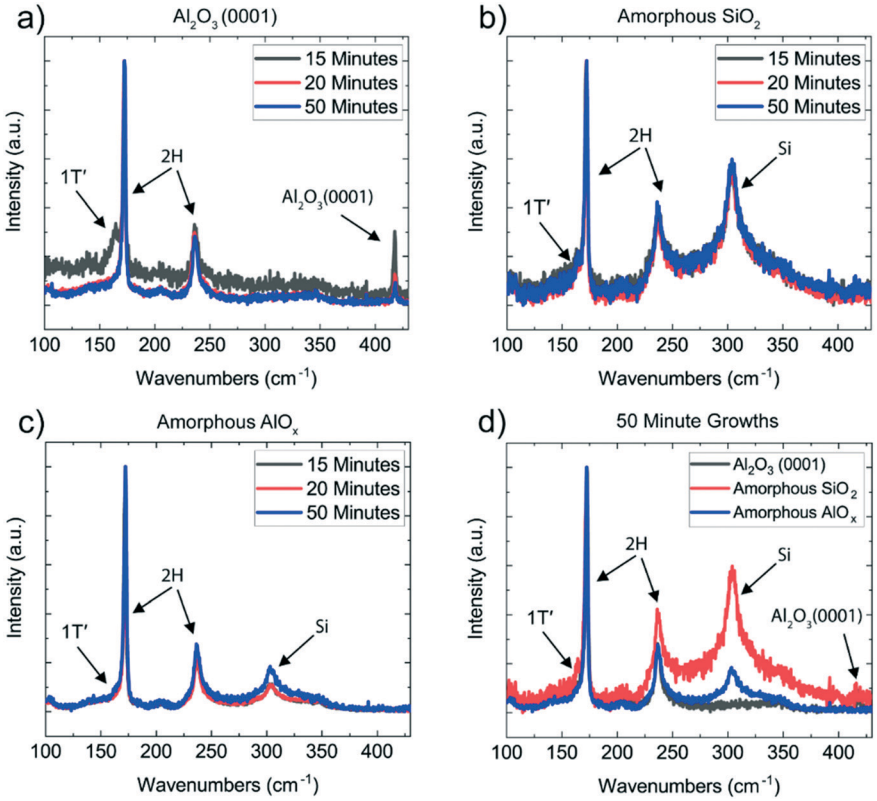

Fig. 2 Raman spectroscopy characterization of $MoTe_2$ films converted on different substrates at varying reaction times. Raman spectra of $MoTe_2$ converted from 8 cycle-thick MoO_x deposited on Al_2O_3 (0001) (a), amorphous SiO_2 (b), and amorphous AlO_x (c). Spectra were captured after three different intervals for each sample: 15 minutes (black), 20 minutes (red), and 50 minutes (blue). Overlaid spectra from all three substrates after 50 minutes of growth are shown in (d).

We note the residual MoO_x is not reflected in the O 1s binding energy, which is dominated by the oxygen of the underlying substrates (Fig. S5†). The same result is observed when 10 cycle-thick MoO_x films were converted on the three substrates (Fig. S6†).

We also investigated the topography of the $MoTe_2$ films using atomic force microscopy (AFM). Fig. 4 shows the changes in topography of $MoTe_2$ as a function of substrate and reaction time. Before the reaction, the surface roughness of the MoO_x films deposited on the three substrates was measured, showing that the Al_2O_3 (0001) case is the most flat and films grown on amorphous AlO_x and SiO_x substrates have higher surface roughness similar to each other. No significant changes were observed in the surface roughness after annealing the MoO_x films in H_2/Ar environment at 600 °C (Fig. S7†). After the conversion to $MoTe_2$, the height distribution profiles show that the surface roughness of $MoTe_2$ on all three substrates is much larger than the initial surface roughness of the substrates (Fig. 4e, j and o), indicating the formation of discontinuous monolayer $MoTe_2$ islands of domain size in the 10's of nm range (Fig. 4d, i and n). This is due to the insufficient number of ALD cycles for the initial MoO_x precursor film for the synthesis of continuous monolayer $MoTe_2$ and could be remedied by increasing the thickness of the MoO_x film.[15] $MoTe_2$ films converted on Al_2O_3 (0001) are the most flat, while $MoTe_2$ films converted on amorphous AlO_x became slightly rougher as the conversion continued from 15 minutes to 50 minutes of reaction time. In contrast, the surface roughness of the $MoTe_2$ on the SiO_2 substrate did not appear to change after the initial 15 minutes of reaction and, after 50 minutes of reaction, the surface roughness of the $MoTe_2$ is the largest on SiO_2. The same trend in surface roughness was observed for $MoTe_2$ films converted from 10 cycle-thick MoO_x films (Fig. S8†).

The Raman and XPS analysis suggest that $MoTe_2$ conversion occurs most quickly on the amorphous AlO_x substrate and most slowly on the amorphous SiO_2 substrate. Additionally, residual MoO_x peaks remain for $MoTe_2$ converted on amorphous substrates, possibly suggesting chemical bonding at the interface between $MoTe_2$ and the substrate. Therefore, from the combination of Raman spectroscopy, XPS, and AFM analysis, we conclude that the chemistry of the substrate has a major role in the nucleation of 2H monolayer $MoTe_2$ films from precursor MoO_x films. One reason this could occur is the overall diffusivity of the MoO_x films on SiO_2 *vs.* AlO_x. It has been shown previously that MoO_x shows greater diffusivity on amorphous AlO_x than it does on amorphous SiO_2,[21] indicating stronger wetting between MoO_x and AlO_x. Growth of other TMDCs on AlO_x

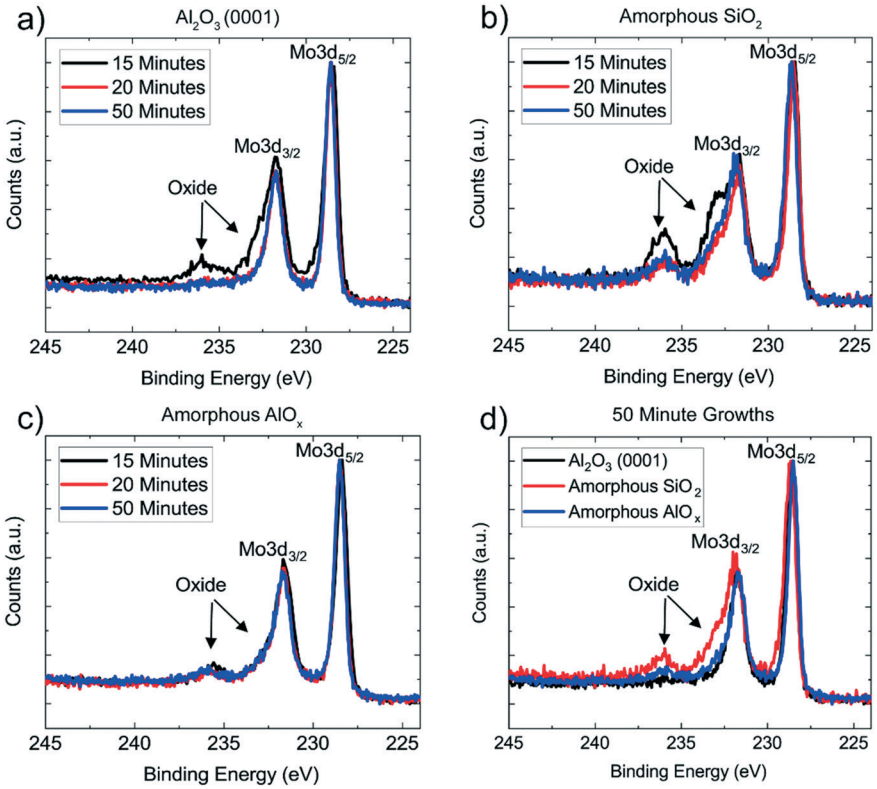

Fig. 3 XPS analysis of Mo 3d peaks in $MoTe_2$ films converted on different substrates at varying reaction times. XPS of Mo 3d peaks in $MoTe_2$ films converted from 8 cycle-thick MoO_x deposited on Al_2O_3 (0001) (a), amorphous SiO_2 (b), and amorphous AlO_x (c). Spectra were captured after three different intervals for each sample: 15 minutes (black), 20 minutes (red), and 50 minutes (blue). Overlaid spectra from all three substrates after 50 minutes of growth are shown in (d).

and SiO_x substrates has also been examined. When WS_2 was synthesized directly on different substrates by ALD using WF_6 and H_2S as precursors, the Delabie group at University of Leuben showed that WS_2 on amorphous AlO_x and sapphire Al_2O_3 grew in a layer-by-layer manner,[22] while WS_2 on amorphous SiO_2 grew in a 3D manner as clusters.[23] Their results suggest that the W precursor interacts more strongly with sapphire Al_2O_3 or AlO_x than with SiO_2, similar to the diffusivity case of MoO_x on AlO_x *vs.* SiO_2. Additionally, it has been shown that adhesion of metal atoms to oxide supports depends more strongly on the choice of oxide support rather than the metal.[24] Thus, these studies provide strong evidence that the conformal synthesis of 2D materials on AlO_x *vs.* SiO_x substrates is driven by better adhesion between metal atoms (Mo or W) and the oxide substrates underneath, as opposed to crystallinity of the substrates. We also note that strain imparted from the substrate due to different degrees of thermal expansion could stabilize the 1T′ phase over the 2H phase. It has been shown that CVD grown WSe_2 on SiO_2 experience significant tensile strain due to a large mismatch between the thermal expansion coefficient values, while WSe_2 grown on sapphire experience little strain due to similar thermal expansion coefficients.[25] This could be significant as the phase transition of $MoTe_2$ is sensitive to strain.[26] In addition to the effect of substrate composition on the nucleation and film uniformity of $MoTe_2$, we further observe that substrate crystallinity affects the bonding at the interface between $MoTe_2$ and substrate: MoO_x is present at the interface between $MoTe_2$ and amorphous AlO_x while it is absent between $MoTe_2$ and crystalline Al_2O_3. Although a relationship has been determined for $MoTe_2$ on the three different substrates, conclusive physical explanations for why adhesion energies of metal atoms on different oxide substrates are different are unclear.[24]

Conclusion

While large-area synthesis of $MoTe_2$ thin films has been demonstrated previously, the impact of chemistry and crystallinity of the substrate on the nucleation and crystalline quality of $MoTe_2$ has been unclear. Here, we show that the conversion of MoO_x to monolayer 2H $MoTe_2$ proceeds at comparable rates on amorphous AlO_x and Al_2O_3 (0001), while the conversion is slower on SiO_2. We conclude that this is due to increased wetting between Te or Mo atoms on the surface of AlO_x compared to SiO_x, allowing for improved lateral mobility and reconfiguration to successfully realize the 2H phase. This work shows the need for further studies regarding substrate interactions during synthesis of 2D materials and for increased understanding of the diffusion of metal species on oxide films.

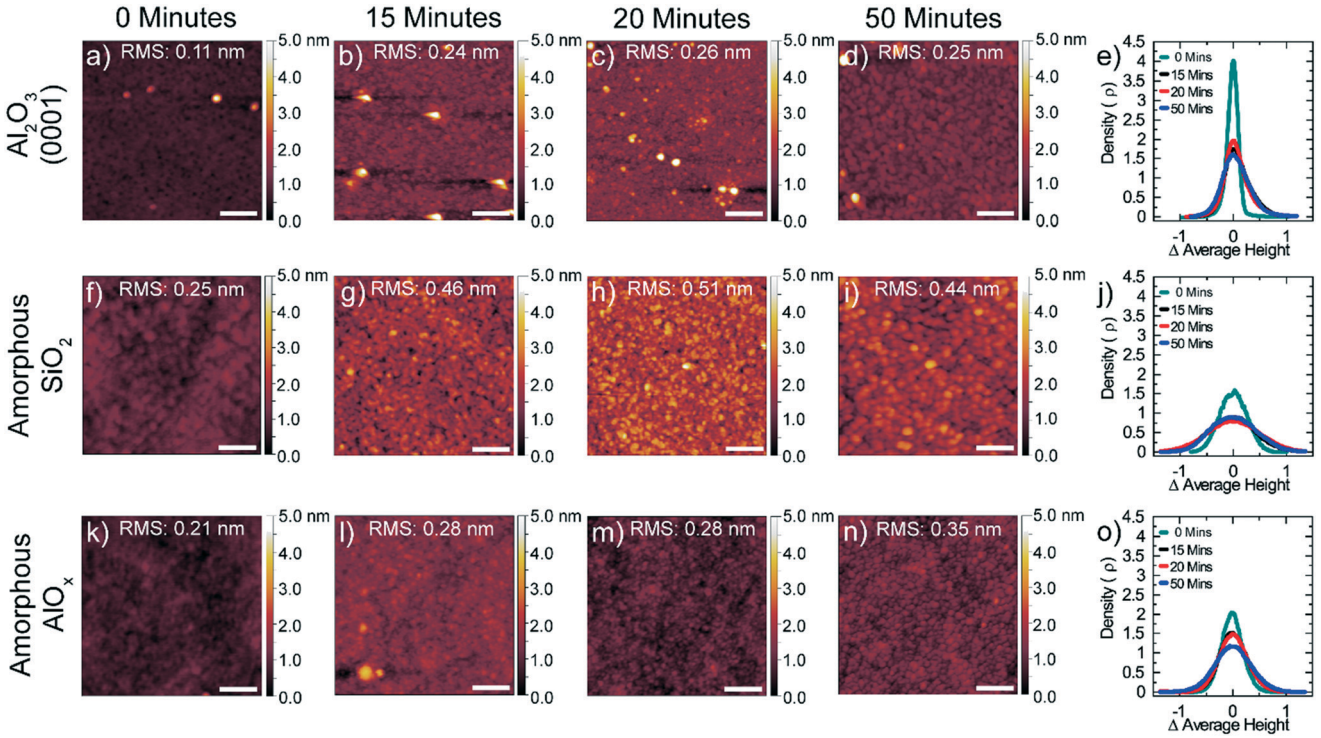

Fig. 4 AFM characterization of $MoTe_2$ films converted on different substrates at varying reaction times. AFM images of $MoTe_2$ converted from 8 cycle-thick MoO_x deposited on Al_2O_3 (0001) (a–d), amorphous SiO_2 (f–i), and amorphous AlO_x (k–n) after different reaction times. Scale bars, 100 nm. Height profiles for the three substrates (e, j and o) were obtained by averaging the height distributions of four AFM images taken from each sample, 8 μm distance from one another at each time point: 0 minutes (cyan, pristine oxide), 15 minutes (black), 20 minutes (red), and 50 minutes (blue).

Methods

Atomic layer deposition of MoO_x films and substrate preparation

Silicon wet thermal oxide substrates (500 nm, University Wafer) were prepared using a standard RCA process. Samples were immersed in a 5 : 1 : 1 volume ratio solution of deionized (18 MΩ) H_2O (18.2 MΩ) : NH_4OH : H_2O_2 and subsequently immersed in a 6 : 1 : 1 solution of DI H_2O : HCl : H_2O_2. Both rinses were conducted for 10 min between 70 and 80 °C and were immediately followed by a DI H_2O rinse.

Atomic layer deposition of 3 nm thick AlO_x films was performed in a Cambridge Nanotech S-100 reactor at a substrate temperature of 200 °C. The silicon thermal oxide substrates (500 nm, University Wafer) were first pretreated with UV-ozone for 2 minutes. Trimethylaluminum (TMA) and O_3 were utilized as precursors for 30 cycles of ALD, giving approximately 3 nm of amorphous AlO_x on the surface of the thermal oxide substrate.

Sapphire substrates were cleaned in a modified version of the RCA process.[27] The first step was a soak in an ethanol bath for 12 hours at room temperature, followed by a rinse with DI H_2O. Samples were then sonicated for 30 min at room temperature in a 1 : 20 : 79 solution of detergent : ethanol : DI H_2O. Samples were then soaked in a 3 : 1 H_2SO_4 : H_2O_2 piranha solution. Finally, samples were immersed in more concentrated variants of the standard RCA solutions, comprising 2 : 1 : 1 DI H_2O : NH_4OH : H_2O_2 and 2 : 1 : 1 DI H_2O : HCl : H_2O_2. Each of the latter 3 rinses was conducted for 20 min at 80 °C and was followed with a DI H_2O rinse. All samples were dried with high purity nitrogen gas between each step.

Atomic layer deposition of MoO_x films was performed in a Cambridge Nanotech S-100 reactor at a substrate temperature of 200 °C. Bis(*tert*-butylimido)bis(dimethylamido)molybdenum $(NtBu)_2(NMe_2)_2Mo$ and ozone were utilized as precursors in accordance with a previously published procedure.[28] Films of different thicknesses were synthesized using cycle numbers of 8, 10, and 120.

Conversion of MoO_x to $MoTe_2$ films

$MoTe_2$ thin films were synthesized through the annealing of MoO_x thin films of various thicknesses grown by ALD in a tellurium atmosphere. Te powder (2 g, Sigma-Aldrich, 99.999%) was placed in a 2 inch quartz tube at zone 1 of a two-zone furnace (MTI OTF-1200X-II), while MoO_x thin films on various substrates were placed downstream in the second zone of the tube furnace. After purging the tube many times with Ar to ensure no residual oxygen was present, the two zones were heated to 570 °C for Te powder and 600 °C for MoO_x films in 15 min and held there for 50 minutes total, with characterization conducted after 3 different time intervals: 15 minutes, 20 minutes, and 50 minutes. A mixture

of H_2/Ar was flowed at 100/10 sccm in atmospheric pressure during the reaction. After the synthesis was completed, the chamber was purged with 200 sccm Ar gas for 25 minutes, and then rapidly cooled to room temperature by opening the furnace cover. We note that the samples were removed from the furnace for characterization between the three time intervals. Thus, the samples were first reacted for 15 minutes, then for additional 5 minutes (denoted as '20 minutes'), and finally for additional 30 minutes (denoted as '50 minutes').

Structural and chemical characterization

Plan-view TEM images were taken at 200 kV using a Tecnai Osiris microscope at the Yale Institute for Quantum Engineering (YINQE). All plan-view $MoTe_2$ films were grown on amorphous AlO_x substrates for easy lift-off using hydrofluoric acid as etching of sapphire for lift-off was proven difficult and the lifted $MoTe_2$ films were transferred onto carbon covered Quantifoil TEM grids with equally spaced 2 μm holes. To characterize the surface of the films, atomic force microscopy was conducted using a Cypher ES microscope from Asylum Research. The microscope was operated in peak-force tapping mode. Raman spectroscopy (Horiba) was used to verify film uniformity and characterize the thickness and phase of the $MoTe_2$ films. The laser used was 633 nm, with a laser power of 10% and diffraction grating 1800 g mm^{-1}. Full conversion of the films from MoO_x to $MoTe_2$ was verified through X-ray photoelectron spectroscopy (XPS) (PHI VersaProbe II).

Conflicts of interest

There are no conflicts to declare.

Acknowledgements

D. J. H. was supported by the NASA graduate student fellowship #80NSSC19K1131. J. J. C. acknowledges support from DOE BES DE-SC0014476. N. C. S and B. D. acknowledge support from the National Science Foundation Grant No. 1605129. The following user facilities are acknowledged for instrument use, scientific and technical assistance: the Yale West Campus Materials Characterization Core (MCC), the Yale West Campus Imaging Core, and the Yale Institute for Nanoscience and Quantum Engineering (YINQE).

References

1 D. Deng, K. S. Novoselov, Q. Fu, N. Zheng, Z. Tian and X. Bao, Catalysis with Two-Dimensional Materials and Their Heterostructures, *Nat. Nanotechnol.*, 2016, **11**, 218–230.

2 B. Xu, S. Qi, M. Jin, X. Cai, L. Lai, Z. Sun, X. Han, Z. Lin, H. Shao, P. Peng, Z. Xiang, J. E. ten Elshof, R. Tan, C. Liu, Z. Zhang, X. Duan and J. Ma, 2020 Roadmap on Two-Dimensional Materials for Energy Storage and Conversion, *Chin. Chem. Lett.*, 2019, **30**, 2053–2064.

3 X. Xu, S. Chen, S. Liu, X. Cheng, W. Xu, P. Li, Y. Wan, S. Yang, W. Gong, K. Yuan, P. Gao, Y. Ye and L. Dai, Millimeter-Scale Single-Crystalline Semiconducting $MoTe_2$ via Solid-to-Solid Phase Transformation, *J. Am. Chem. Soc.*, 2019, **141**, 2128–2134.

4 Y. Tao, J. A. Schneeloch, C. Duan, M. Matsuda, S. E. Dissanayake, A. A. Aczel, J. A. Fernandez-Baca, F. Ye and D. Louca, Appearance of a T_d* Phase across the T_d-T′ Phase Boundary in the Weyl Semimetal $MoTe_2$, *Phys. Rev. B*, 2019, **100**, 100101(R).

5 C. Heikes, I. L. Liu, T. Metz, C. Eckberg, P. Neves, Y. Wu, L. Hung, P. Piccoli, H. Cao, J. Leao, J. Paglione, T. Yildirim, N. P. Butch and W. Ratcliff, Mechanical Control of Crystal Symmetry and Superconductivity in Weyl Semimetal $MoTe_2$, *Phys. Rev. Mater.*, 2018, **2**, 074202.

6 Y. Qi, P. G. Naumov, M. N. Ali, C. R. Rajamathi, W. Schnelle, O. Barkalov, M. Hanfland, S.-C. Wu, C. Shekhar, Y. Sun, V. Sü, M. Schmidt, U. Schwarz, E. Pippel, P. Werner, R. Hillebrand, T. Förster, E. Kampert, S. Parkin, R. J. Cava, C. Felser, B. Yan and S. A. Medvedev, Superconductivity in Weyl Semimetal Candidate $MoTe_2$, *Nat. Commun.*, 2016, **7**, 11038.

7 S. Cho, S. H. Kang, H. S. Yu, H. W. Kim, W. Ko, S. W. Hwang, W. H. Han, D. Choe, Y. H. Jung, K. J. Chang, Y. H. Lee, H. Yang and S. W. Kim, Te Vacancy-Driven Superconductivity in Orthorhombic Molybdenum Ditelluride, *2D Mater.*, 2017, **4**, 021030.

8 W. Wang, S. Kim, M. Liu, F. A. Cevallos, R. J. Cava and N. P. Ong, Evidence for an Edge Supercurrent in the Weyl Superconductor $MoTe_2$, *Science*, 2020, **368**, 534–537.

9 X. Qian, J. Liu, L. Fu and J. Li, Quantum Spin Hall Effect in Two-Dimensional Transition Metal Dichalcogenides, *Science*, 2014, **346**, 1344–1347.

10 W. Hou, A. Azizimanesh, A. Sewaket, T. Peña, C. Watson, M. Liu, H. Askari and S. M. Wu, Strain-Based Room-Temperature Non-Volatile $MoTe_2$ Ferroelectric Phase Change Transistor, *Nat. Nanotechnol.*, 2019, **14**, 668–673.

11 Y. Wang, J. Xiao, H. Zhu, Y. Li, Y. Alsaid, K. Y. Fong, Y. Zhou, S. Wang, W. Shi, Y. Wang, A. Zettl, E. J. Reed and X. Zhang, Structural Phase Transition in Monolayer $MoTe_2$ Driven by Electrostatic Doping, *Nature*, 2017, **550**, 487–491.

12 C. Zhang, S. KC, Y. Nie, C. Liang, W. G. Vandenberghe, R. C. Longo, Y. Zheng, F. Kong, S. Hong, R. M. Wallace and K. Cho, Charge Mediated Reversible Metal–Insulator Transition in Monolayer $MoTe_2$ and $W_xMo_{1-x}Te_2$ Alloy, *ACS Nano*, 2016, **10**, 7370–7375.

13 M. J. Mleczko, A. C. Yu, C. M. Smyth, V. Chen, Y. C. Shin, S. Chatterjee, Y. C. Tsai, Y. Nishi, R. M. Wallace and E. Pop, Contact Engineering High-Performance n-Type $MoTe_2$ Transistors, *Nano Lett.*, 2019, **19**, 6352–6362.

14 N. R. Pradhan, D. Rhodes, S. Feng, Y. Xin, S. Memaran, B. H. Moon, H. Terrones, M. Terrones and L. Balicas, Field-Effect Transistors Based on Few-Layered α-$MoTe_2$, *ACS Nano*, 2014, **8**, 5911–5920.

15 D. J. Hynek, R. M. Singhania, S. Xu, B. Davis, L. Wang, M. Yarali, J. V. Pondick, J. M. Woods, N. C. Strandwitz and J. J.

Cha, Cm^2-Scale Synthesis of $MoTe_2$ Thin Films with Large Grains and Layer Control, *ACS Nano*, 2021, **15**, 410–418.

16 C. Ruppert, O. B. Aslan and T. F. Heinz, Optical Properties and Band Gap of Single- and Few-Layer $MoTe_2$ Crystals, *Nano Lett.*, 2014, **14**, 6231–6236.

17 M. Grzeszczyk, K. Gołasa, M. Zinkiewicz, K. Nogajewski, M. R. Molas, M. Potemski, A. Wysmołek and A. Babiński, Raman Scattering of Few-Layers $MoTe_2$, *2D Mater.*, 2016, **3**, 025010.

18 Q. J. Song, Q. H. Tan, X. Zhang, J. B. Wu, B. W. Sheng, Y. Wan, X. Q. Wang, L. Dai and P. H. Tan, Physical Origin of Davydov Splitting and Resonant Raman Spectroscopy of Davydov Components in Multilayer $MoTe_2$, *Phys. Rev. B*, 2016, **93**, 115409.

19 J. Wang, X. Luo, S. Li, I. Verzhbitskiy, W. Zhao, S. Wang, S. Y. Quek and G. Eda, Determination of Crystal Axes in Semimetallic T′-$MoTe_2$ by Polarized Raman Spectroscopy, *Adv. Funct. Mater.*, 2017, **27**, 1604799.

20 J.-H. Huang, H.-H. Hsu, D. Wang, W.-T. Lin, C.-C. Cheng, Y.-J. Lee and T.-H. Hou, Polymorphism Control of Layered $MoTe_2$ through Two-Dimensional Solid-Phase Crystallization, *Sci. Rep.*, 2019, **9**, 8810.

21 W. Xu, J. Yan, N. Wu, H. Zhang, Y. Xie, Y. Tang, Y. Zhu and W. Yao, Diffusing Behavior of MoO_3 on Al_2O_3 and SiO_2 Thin Films, *Surf. Sci.*, 2000, **470**, 121–130.

22 B. Groven, A. N. Mehta, H. Bender, Q. Smets, J. Meersschaut, A. Franquet, T. Conard, T. Nuytten, P. Verdonck, W. Vandervorst, M. Heyns, I. Radu, M. Caymax and A. Delabie, Nucleation Mechanism during WS_2 Plasma Enhanced Atomic Layer Deposition on Amorphous Al_2O_3 and Sapphire Substrates, *J. Vac. Sci. Technol., A*, 2018, **36**, 01A105.

23 B. Groven, A. Nalin Mehta, H. Bender, J. Meersschaut, T. Nuytten, P. Verdonck, T. Conard, Q. Smets, T. Schram, B. Schoenaers, A. Stesmans, V. Afanas'Ev, W. Vandervorst, M. Heyns, M. Caymax, I. Radu and A. Delabie, Two-Dimensional Crystal Grain Size Tuning in WS_2 Atomic Layer Deposition: An Insight in the Nucleation Mechanism, *Chem. Mater.*, 2018, **30**, 7648–7663.

24 S. L. Hemmingson and C. T. Campbell, Trends in Adhesion Energies of Metal Nanoparticles on Oxide Surfaces: Understanding Support Effects in Catalysis and Nanotechnology, *ACS Nano*, 2017, **11**, 1196–1203.

25 G. H. Ahn, M. Amani, H. Rasool, D. H. Lien, J. P. Mastandrea, J. W. Ager, M. Dubey, D. C. Chrzan, A. M. Minor and A. Javey, Strain-Engineered Growth of Two-Dimensional Materials, *Nat. Commun.*, 2017, **8**, 608.

26 S. Song, D. H. Keum, S. Cho, D. Perello, Y. Kim and Y. H. Lee, Room Temperature Semiconductor–Metal Transition of $MoTe_2$ Thin Films Engineered by Strain, *Nano Lett.*, 2016, **16**, 188–193.

27 D. Zhang, Y. Wang and Y. Gan, Characterization of Critically Cleaned Sapphire Single-Crystal Substrates by Atomic Force Microscopy, XPS and Contact Angle Measurements, *Appl. Surf. Sci.*, 2013, **274**, 405–417.

28 A. Bertuch, G. Sundaram, M. Saly, D. Moser and R. Kanjolia, Atomic Layer Deposition of Molybdenum Oxide Using Bis(Tert-Butylimido)Bis(Dimethylamido) Molybdenum, *J. Vac. Sci. Technol., A*, 2014, **32**, 01A119.